Assessment of Steel Pipe-shaped Structure under Blast Loading: A Benchmark and Parametric Study Using Finite Element Approach

M. Iqbal Maulana [1], Aditya Rio Prabowo [1,*], Teguh Muttaqie [2], Nurul Muhayat [1], Quang Thang Do [3], Muhammad Imaduddin Hanif [1], and Mufti Reza Aulia Putra [4]

[1] Department of Mechanical Engineering, Universitas Sebelas Maret, Surakarta, Indonesia
[2] Research Center for Hydrodynamics Technology, National Research and Innovation Agency (BRIN), Surabaya, Indonesia
[3] Department of Naval Architecture and Ocean Engineering, Nha Trang University, Nha Trang, Vietnam
[4] Department of Electrical Engineering, Universitas Sebelas Maret, Surakarta, Indonesia
Email: iqbalmaulana@student.uns.ac.id (M.I.M.); aditya@ft.uns.ac.id (A.R.P.); teguh.mutaqie@brin.go.id (T.M.); nurulmuhayat@staff.uns.ac.id (N.M.); thangdq@ntu.edu.vn (Q.T.D.); hanifimad23@student.uns.ac.id (M.I.H.); muftireza@staff.uns.ac.id (M.R.A.P.)
*Corresponding author

***Abstract*—Steel is the main material in the industrial sector. The material must have high strength to withstand explosive forces or loads that can occur at any time. Accidents are inevitable if no countermeasures or forecasts can be used as a reliable reference for designing mitigation or evacuation plans. To avoid such accidents, this research aims to develop a pipe structure that has high structural resistance to explosive loading that may occur due to internal explosions in the pipe. The research method used is the simulation method to determine how the structure responds to the blast load and how much deflection occurs in the structure at each load variation. This research was designed and tested using finite element analysis in ABAQUS/Explicit. Validation of the simulation was carried out with a comparative study of the pioneer experimental results. Analyses were conducted with numerical parameters (TNT loading and mesh size variation) and physical parameters (material variation). The analysis results showed that numerical parameters (mesh variation) affected the accuracy of simulation data, while physical parameters affected the performance of steel pipe shaped structures.**

***Keywords*—steel, steel pipe-shaped structure, blast loading, finite element method**

I. Introduction

The steel industry is the mother of all industries, which means that the steel industry has a vital role in developing the manufacturing and construction industries in the context of national economic growth [1]. Steel is also a supplier of raw materials for other industrial sectors. Steel is a critical material in all industrial sectors such as construction, automotive, shipping, electronics, machinery, tools, oil and gas, power plants, telecommunications, food and beverage can industry. Indonesia has many iron ore resources, such as raw materials for pellets, sponge iron, and others, spread across several provinces. Initially, the development of the steel industry in Indonesia was prioritized to meet steel needs for infrastructure development such as; roads, bridges, office buildings, markets, houses, and other buildings. Along with the increase in population, technological developments, and increasing demand for various types of steel, such as household needs and household offices and offices, motor vehicle industry, defense industry (armament industry, combat vehicles, and submarines), the demand for various types of steel also continues to increase [2].

Because steel is a crucial material in the industrial sector, it must have high strength to withstand explosive forces or loads that can occur at any time. Recently, much research has been conducted on the response of geometric structures to accidental collisions and loads [3–7], including the loading of air blasts [8, 9]. Explosives are chemically or energy-unstable materials, or they can produce a sudden expansion of the material followed by the onset of heat and a significant change in pressure (and usually also a large flash or sound), known as an explosion [10]. This sudden release of energy occurs over a very short period of time (microsecond scale). Explosion, according to Beyle [11], is the sudden conversion of potential energy (chemical or mechanical) into kinetic energy by the production and release of gas under pressure or the release of gas under pressure. This high-pressure gas performs mechanical work such as moving, altering, or destroying nearby material. One of the most widely used military high-explosive materials, partly because of its insensitivity to shock and friction, is Trinitrotoluene, or TNT. Trinitrotoluene, or TNT, is a pale yellow solid organic nitrogen compound with $C_6H_2(NO_2)_3CH_3$ formula.

Manuscript received July 13, 2023; revised August 10, 2023; accepted August 24, 2023; published January 26, 2024.

TNT has the IUPAC (International Union of Pure and Applied Chemicals) name 2-methyl-1, 3, 5–Trinitrobenzene. It has a molecular weight of 227.13 g/mol, corresponding to the total number of atomic weights that compose it [12]. Because of its safe and easy use, TNT is widely used as an explosive in the military industry. The possibility of spontaneous or accidental explosions in TNT is also very small due to its high melting point and insensitivity to shock.

In view of this, research into the scenario of steel pipe-shaped structures against explosion needs to be carried out to study the damage that may occur and is one of the efforts to overcome similar incidents that may recur due to damage to the pipe. With today's technology, many software or computer programs can be used to accurately model the behaviour of materials or structural components using the principles of the finite element method. ABAQUS® Finite Element Method (FEM) software was used to model a cylindrical pipe subjected to TNT loading and varying materials.

This research aims to develop a pipe structure that has high structural resistance to explosive loading that may occur due to internal explosions in the pipe. The research was conducted by simulating TNT loading on the pipe structure, which was validated through a benchmarking process against experimental testing. Variations in the numerical and physical parameters of the pipe structure were included to determine the design of the pipe structure with optimal explosion resistance performance.

II. Literature Review

Experiments on TNT explosion loading in simulation and experimentation have been conducted by several previous researchers. Several types of research on air blasts have been conducted in simulation using software and experiments due to the limitations of each method. Chi *et al.* [13] investigated the type of soil used in buried pipes greatly affects the mechanical properties of the pipes. The results show that API X80 material performs better in terms of burst load, compared to X42, X52, X65, and X70 if other parameters remain the same. The addition of soil type variation can still be given as one of the variations for future research. Wu *et al.* [14] investigated the structural response behaviour of high-density polyethylene pipes experimentally and numerically. Experimental analysis shows that the Peak Particle Velocity (PPV) of the pipe and surface increases as the distance from the explosive decreases, and the vibration velocity of all measurement points is dominated by the vertical direction. The numerical simulation results also show corresponding results with different damage levels related to the explosive charge and distance from the explosive. Elveli *et al.* [15] evaluated the effects of a complex, partially confined explosion on thin steel plates with pre-formed defects by experimental methods and numerical studies. Experimental results showed a decrease in fracture resistance during blast loading. Simulation results showed excellent correlation with respect to center point deflection and deformation profile. The addition of other material variations and explosive loading is still possible for future research. Song *et al.* [16] examined the dynamic response of X70 grade steel pipe under localised blast loading through experimental and numerical investigations. The experimental results showed the deflection and damage rate of the pipe increase with the increase of explosive mass and contact area. The wall thickness plays an important role on the damage and post-failure motion. The numerical simulation results show a good correlation with the experiments. For future research, it is still possible to add material variations and geometry variations such as providing stiffeners or rings at the edge of the pipe. Henchie *et al.* [17] conducted experimental and numerical investigations of the response of circular Domex-700 MC steel plates to repeated uniform blast loads. The experimental results showed a decrease in the center point deflection and an increase in the Vickers hardness of the plate at the boundary and center regions with increasing amounts of blast load. Simulation results show excellent correlation with respect to center point deflection and deformation profile. The addition of other material variations and blast loading is still possible for future research. Karagiozovaa *et al.* [18] investigated the energy absorption of round and square aluminium alloy tubes that have been subjected to axial blast loads, which are transmitted to the tubes by a small mass. The results showed material properties play an important role in the formation of buckling patterns. The increase of energy absorption capacity in the case of the increased load is affected by the shell under a large blast load, thus causing high-speed axial impact. Geometry variations such as thickness in the walls of cylindrical and square pipes are still possible to research in the future.

The explosion phenomena and structural response of pipelines under explosive loading that occurred both in theory, laboratory experiments, and finite element method in the marine sector were studied by [19–22]. Zhu *et al.* [19] investigated the response of polyurea-coated tubular concrete structures to blast loads. The results showed that polyurea coated on the back or both sides of aluminum plates can improve blast resistance. The type of material used by Zhu is limited to Al Alloy 6065-T5. The use of other materials is still possible for future research. Kristoffersen *et al.* [20] investigated the structural response of a standard tubular concrete pipe using active explosives with three different positions for the explosive charge and varied charge sizes. The experimental results showed that contact charges detonated from the outside require about twice the number of blasts to penetrate the pipe than contact charges detonated from the inside, which shows a significant confinement effect. Trials in confined environments such as underwater can still be conducted as a comparison for further research. Sun *et al.* [21] investigated the damage to Q345B steel round tubes due to the combined action of fire and explosion. The results showed that temperature significantly impacts the mechanical properties of steel materials. Variations in the explosive loading of TNT and the type of steel material can still be carried out for future research. Patnaik *et al.* [22] evaluated X70 grade steel pipe against underground blast was carried out numerically. The results showed that

CFRP used as armour on X70 grade steel pipe proved to be able to limit the peak value of displacement, and reduce the pressure in the pipe due to the blast effect. For future research, it is still possible to add material variations. This research is based on experimental research that has been carried out [23] at the University of Liverpool where a 9.5 mm thick open steel pipe with an outer diameter of 324 mm was given a blast load at the center of the open steel pipe.

III. Theoretical Basis

A. Steel Pipe

Pipelines have been used extensively in the world to transport petroleum, natural gas, ammonia, etc., and they play an important role in urban energy distribution [13]. Pipe is defined as a circular tubular product used to convey fluids (liquids, gases, and fluidized solids). Pipes are designed for specific design pressures that correspond to design temperatures. Different types of pipes are used in the industrial sector for different purposes. All piping shall be designed and fabricated in such a way as to ensure the safety of the plant operator, plant, community, and environment [24]. Pipes are usually classified based on the material used to manufacture the pipe manufacture. In general, there are two types of pipes, namely metal pipes and non-metallic pipes. Pipes made of metal are known as metal pipes. They can be grouped into two categories, namely Pipes made of ferrous materials (e.g., steel pipes) and pipes made of non-ferrous materials (e.g., Copper-Nickel). A steel pipe is a cylindrical tube made of steel that is used in a variety of ways in manufacturing and infrastructure. Non-metallic pipe is widely used for services where the temperature is not significant, non-critical services such as industrial water and drainage systems use mostly non-metallic pipe. Common and widely used non-metallic pipes are HDPE pipes, PVC pipes, ABS pipes, etc. Fig. 1 shows the piping system in the industrial sector.

Fig. 1. Piping system in the industrial sector [24].

B. Air Blast Overpressures (ABO)

The explosion releases a large amount of chemical potential energy into the surrounding air through heat and shock waves. Shock waves can be categorized into two groups depending on their intensity and speed. The first is detonation, defined as an intense shock wave propagating at supersonic speeds due to high-pressure gases expanding away from the center of the explosion and compressing the surrounding air. The second wave is deflagration, defined as a widespread shock wave, a relatively small shock wave propagating at subsonic speeds associated with slow mass and heat transfer. The intensity of excess peak pressure caused by deflagration is much smaller than detonation [25]. Lightning creates a cylindrical arc channel, and its shock wave propagates at supersonic speeds as high as Mach 10 [26]. Therefore, lightning-induced shock waves can be idealized as those caused by detonation. Similar to lightning, when an explosion occurs, a large amount of chemical potential energy instantly heats and compresses the surrounding air. The rapid expansion of the detonation product creates hot, dense, high-pressure shock waves known as Air Blast Overpressures (ABO). ABO propagates radially outward from the center of the explosive source to the vicinity [25]. In the modern era like now, explosions can be simulated using theoretical and numerical approaches. The two most popular approaches to calculating Air Blast Overpressure (ABO) are the CONWEP air blast and the CEL model. However, explosion simulations will be conducted using the CONWEP model in this simulation. Fig. 2 shows a pressure-time graph of the blast wave.

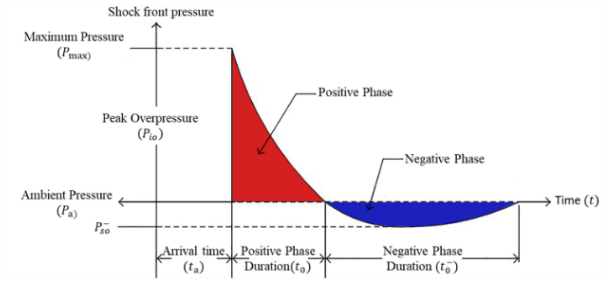

Fig. 2. Pressure-time graph of blast wave.

The initial shock front pressure is equal to the ambient pressure (P_a). The time it takes for the shock wave to propagate from the center of the explosion to the target structure indicates the time of arrival (t_a). Because the shock wave propagates at supersonic speed, the time the shock wave arrives the time it arrives the shock wave is very small. When the shock wave meets the target surface, the incident wave undergoes a pressure jump (increasing with a very small rise time) to the maximum value (P_{max}). The difference between maximum pressures (P_{max}) dan ambient pressure(P_a) defined as peak overpressure (P_{io}) or ABO. The expansion speed of the shock wave and the corresponding overpressure both decrease with time. After reaching the peak value on time t_a, the shock front pressure that occurs decays exponentially back to P_a and followed by a negative phase (smaller than P_a). The time duration of the positive and negative phases is defined as t_0 and t_0^-. The negative phase is usually less important than the positive phase because the structural damage caused by air blasts mostly occurs in the early stages of shock wave generation [27]. The Friedlander equation [28] is used to mathematically represent the positive phase of ABO with exponential decay as follows:

$$P_{io}(t) = (P_{so} - P_a)\left(1 - \frac{t-t_a}{t_0}\right) e^{-\left\{\beta\frac{t-t_a}{t_0}\right\}} \quad (1)$$

where are P_{max}, P_a, t_a, and t_0 respectively represent maximum overpressure, ambient pressure, arrival time, and positive time duration, and β is a dimensionless decay coefficient.

Trinitrotoluene, or TNT, is a pale yellow solid organic nitrogen compound that is one of the most widely used military *high-explosive* materials, partly because of its insensitivity to shock and friction [12]. TNT has been used extensively in the manufacture of explosives since the early 20th century and is used in military shell casings, bombs, and grenades. In the ABAQUS CAE application, the mass of TNT is inputted through interaction *properties* where in the menu can be determined the mass of TNT with some unit conversion adjustments.

C. CONWEP Method

Nuclear, chemical, and biological weapons are notorious for causing large-scale mass destruction. Those weapons that do not cause such large-scale mass destruction, but are capable of causing significant damage to life and property, are generally referred to as conventional weapons/ConWep [29]. These weapons usually include landmines, non-nuclear bombs, bullets, rockets, missiles, etc. The threat from such weapons is measured by the mass of the explosive or the mass of the charge; and blast distance from vulnerable structures or deadlock distance. The mass of a payload used in conventional weapons is usually measured in kilograms of TNT. In ABAQUS software, CONWEP is an empirical equation used to calculate the pressure of a shock wave acting on a surface by considering the mass of TNT for its explosive charge [25]. According to Hopkinson-Cranz, the law of scale can be used to correlate the effects of proximity to the center of the explosion and the weight of the explosive charge on shock wave generation [25]. The law of distance scale (Z) is defined in Eq. (2).

$$Z = \frac{R}{W^{\frac{1}{3}}} \quad (2)$$

where, R is the stand-off distance, which is the distance from the center of the explosion to the target surface. The farther the center of the explosion is from the surface, the less structural damage is caused by the blast wave. W is the weight of the explosive charge.

Total air blast overpressure (P_{total}) is obtained by combining the incidence angle (θ) depending on the incidence of overpressure (P_{io}) and reflected overpressure (P_{ro}). The total air blast overpressure is defined in Eqs. (3)–(5).

$$P_{total}(t) = \begin{cases} [P_{ro}(t) - 2P_{io}(t)]\cos\theta^2 + [\cos\theta + 1]P_{io}(t), \cos\theta \geq 0 \\ P_{io}(t), \cos\theta < 0 \end{cases} \quad (3)$$

$$P_{io}(t) = (P_{so} - P_a)\left(1 - \frac{t-t_a}{t_0}\right) e^{-\left(\beta\frac{t-t_a}{t_0}\right)}, \quad (4)$$

$$P_{ro}(t) = 2P_{io}(t) + \frac{(\gamma+1)\{P_{io}(t)\}^2}{2\gamma P_a + (\gamma-1)P(t)}. \quad (5)$$

where P_{so} shows peak incident pressure. Subscript "so" has been used to indicate peak incident pressure and side pressure. P_a represents ambient pressure; t_a indicates the arrival time of the shock wave propagating to the target structure; t_0 is the time duration of the positive phase; β is a dimensionless decay coefficient that depends on the shape of the shock wavefront; and γ is the specific heat ratio of air [27].

D. Johnson-Cook Model

The Johnson-Cook (J-C) constitutive model is widely used in finite element simulation, as it shows the relationship between stress and strain in a simple way. The Johnson-Cook (J-C) constitutive model is one of many semi-empirical constitutive models describing the behavior of plastic materials at high strain, strain rates, and high temperatures that is most widely used due to its simple but effective performance [30–34]. Using the Johnson-Cook model, the stress flow of a material can be expressed using the equation as shown in Eq. (6).

$$\sigma = (A + B\varepsilon^n)\left(1 + C\ln\left(\frac{\dot{\varepsilon}}{\dot{\varepsilon_0}}\right)\right)\left[1 - \left(\frac{T-T_r}{T_m-T_r}\right)^m\right] \quad (6)$$

where σ is the equivalent voltage, and ε is the equivalent plastic strain, $\dot{\varepsilon}$ and ε_0 are the strain rate and the reference strain rate respectively. T, T_m, and T_r each is the actual temperature of the material, the melting point of the material, and the reference temperature (usually set to room temperature). The material constant is A, B, n, C and m. A is the material's yield stress under reference conditions, B is a strain hardening constant, n is the strain hardening coefficient, C is the strain rate reinforcement coefficient, and m is the coefficient of thermal softening. In some finite element simulations, such as ABAQUS software, T_r replaced by T_t (temperature transition) that does not depend on temperature but is present in the voltage response.

IV. Benchmark and Validation

A. Benchmarking: Experiment Reference Profile

The research that will be used as an experimental reference is experimental testing conducted by Rushton *et al.* [23] at the University of Liverpool. The research conducted by Rushton was carried out using an open-ended pipe hung on a support pole and sling, then at the midpoint of the pipe was charged with a cylindrical explosive with a detonator, as shown in Fig. 3.

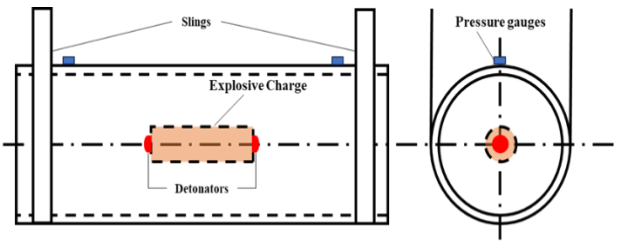

Fig. 3. Experimental setup test by Rushton *et al.* [23].

Some various materials and shapes can be used as energy-absorbing structures. Mild steel is a ferrous metal

made of iron and carbon. Mild steel is an inexpensive material with properties suitable for most engineering applications. In the research reference, open pipe structure, the material used is API-5L-X42 mild steel. The experimental results conducted by Rushton showed a comparison of the power model and experimental data points based on the plastic circle strain for different load masses with the bomb mass comparison based on the reference [23]. The maximum plastic strain graph for different load masses of the material is shown in Fig. 4.

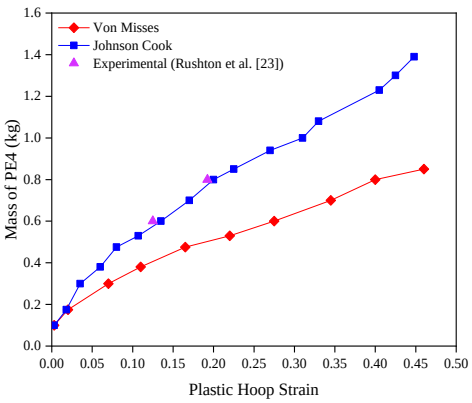

Fig. 4. Maximum plastic strain graph for different loading masses of API-5L-X42 material [23].

Experimental testing was carried out in the laboratory when the pipe was supported horizontally on a support pole and sling. A cylindrical explosive charge will be placed in the center of the pipe with detonators connected at each end at the center of the flat surface. Fig. 5 shows the test cylinder suspended from the sling after internal explosive loading (0.6 kg TNT).

Fig. 5. Test cylinder suspended from sling after internal explosive loading (0.6 kg TNT) [23].

B. Simulation Validation Procedure

The research was conducted by simulation using ABAQUS CAE software. The simulation begins with the validation process of the experiments conducted by Rushton *et al.* [23]. In the validation stage, all the existing settings in the previous study were used to re-model the steel pipe-structure. This was done to ensure that the simulation run was valid and the results are, as mentioned in previous studies, resulting in a standard deviation value below 10%. Thus, the modeling and simulation carried out can be said to be valid, and the results can be accounted for. After the validation process, the research was conducted by simulations of the specified variations. Then continued, with data collection of simulation results from ABAQUS CAE software, the results obtained were analysed. In this research, there were several configurations of the finite element method. The configuration comprised structural geometry, material properties, loading or boundary conditions, and meshing.

C. Experiment vs Numerical Analysis

Validation of simulation testing can be seen by comparing the plastic hoop strain graph in simulation testing with experimental testing. Fig. 6 shows the finite element results of the comparative study conducted with reference to the pipe structure after the explosion (loading of 0.6 kg TNT and 0.8 kg with 0.0025 m meshing).

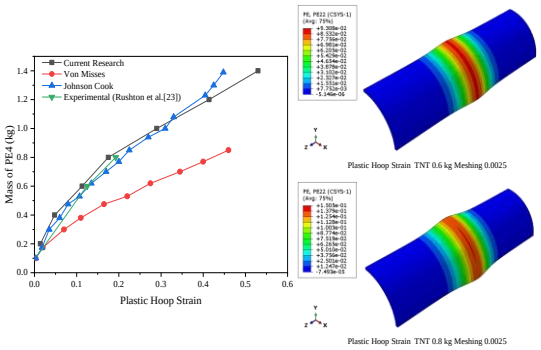

Fig. 6. Comparison of maximum plastic strain from simulation with experiment [23].

Based on the figure above, it can be concluded that the strain value is directly proportional to the additional TNT load. The greater the TNT loading, the greater the strain value. The results of the simulations that have been carried out compared to the experimental data from Rushton show a similar trend so that the validation can be declared satisfactory and successful.

Mesh is a facility to divide and define element types, part types, or assemblies. Convergence calculations are performed on the finite element method analysis for element size selection. The following are the results of the plastic-hoop strain convergence mesh for the pipe structure after the explosion, which are shown in Figs. 7 and 8. The results of the displacement convergence mesh for the pipe structure after the blast are shown in Figs. 9 and 10. From the mesh convergence data, it can be concluded which meshing is the most stable so that it can be used for testing.

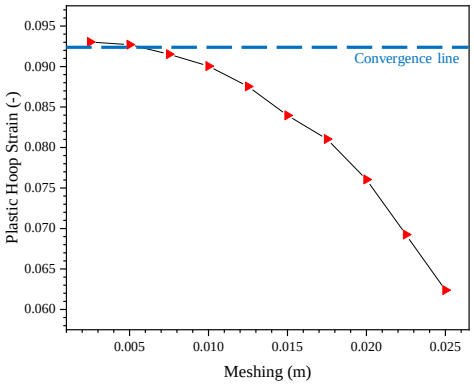

Fig. 7. Mesh – plastic hoop strain curve for TNT 0.6 kg.

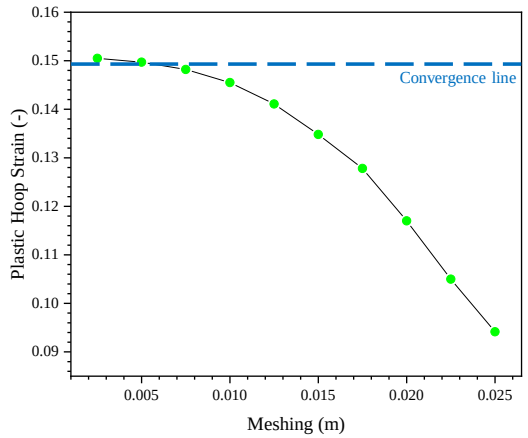

Fig. 8. Mesh – plastic hoop strain curve for TNT 0.8 kg.

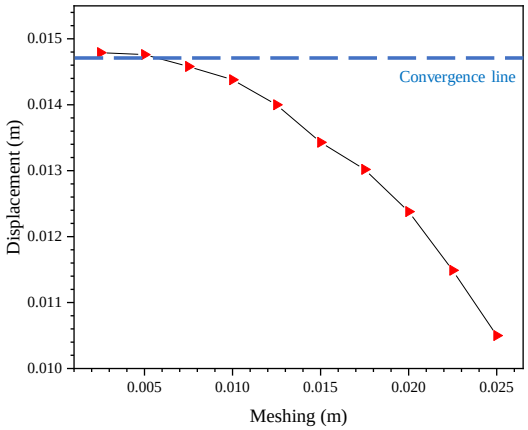

Fig. 9. Mesh – displacement curve for TNT 0.6 kg.

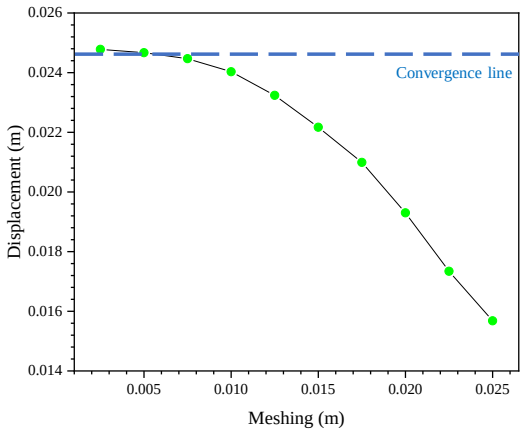

Fig. 10. Mesh – displacement curve for TNT 0.8 kg.

Based on the mesh convergence data for maximum plastic strain-hoop, it can be concluded that the meshing tends to be more stable in terms of the final result, which is between 0.0025 m and 0.0075 m mesh. And based on the mesh displacement data convergence, it can be concluded that the meshing tends to be more stable in terms of the final result, which is between 0.0025 m and 0.0075 m meshing.

V. Parametric Study

The research was conducted in several stages. A literature study of related research studies was conducted in the initial stage. Then design the steel pipe-shaped structure in ABAQUS software. The design at this stage was done by replicating the structure obtained from experiments that had been carried out previously. The validation of experimental results with simulation results was carried out. After getting the appropriate results, the research changed the TNT loading configuration and material. The TNT loading used was 0.6 kg TNT and 0.8 kg TNT. The materials used are API-5L-X42 steel, API-5L-X65 steel, Copper-Nickel alloy (Cu-Ni 90/10), Copper-Nickel alloy (Cu-Ni 70/30), HY-80 steel, and HY-100 steel. The data obtained from the simulation were the values of plastic hoop strain, contour stress, and displacement in each variation. The following are the research stages displayed as a flowchart in Fig. 11.

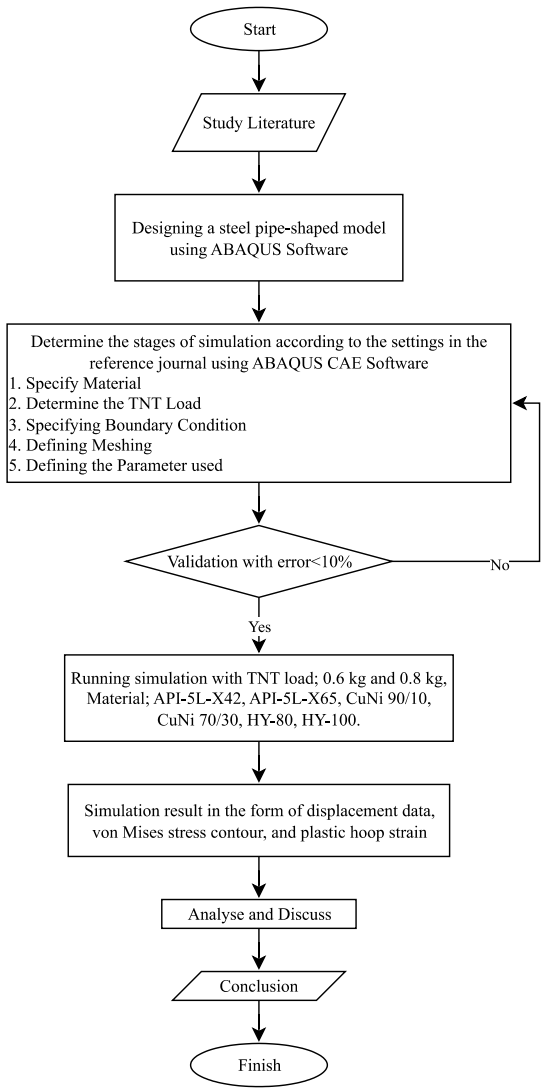

Fig. 11. Flow chart of the current research.

A. Geometrical Model

The experimental reference geometry consists of an open pipe structure geometry. In the experimental profile, an open steel cylinder was suspended from a sling with a

length of 800 mm, a diameter of 324 mm, and a thickness of 9.5 mm. The blast was located 400 mm right in the center of the open steel cylinder. With the pipe open, some of the complicated effects of blast reflections inside the closed vessel would be reduced. The experimental setup test by Rushton *et al.* [23].

B. Material Model

The material model selection was used to obtain the type of material that matched the experiments from the reference, including the structural response due to TNT loading conditions on the material. In reference Rushton *et al.* [21], it is explained that API-5L-X42 mild steel material has mechanical properties as in Table I.

TABLE I. SPECIFICATION OF MILD STEEL USED IN THE EXPERIMENT [23]

Parameter	Value
Density	7850 kg/m^3
Young's Modulus	201 GPa
Poisson's Ratio	0.28
Yield Strength	290 MPa
Ultimate Tensile Strength	413.7 MPa

C. Loading Scheme and Boundary Conditions

The center of the blast loading was placed at a distance of 400 mm, right in the middle of the open steel pipe. The mass of TNT detonated was 0.2 kg–1.4 kg, increasing gradually by 0.2 kg. The open pipe had boundary conditions along the top and bottom of the simulation model. Fig. 12 shows the boundary condition modeling scheme performed in the ABAQUS/CAE software.

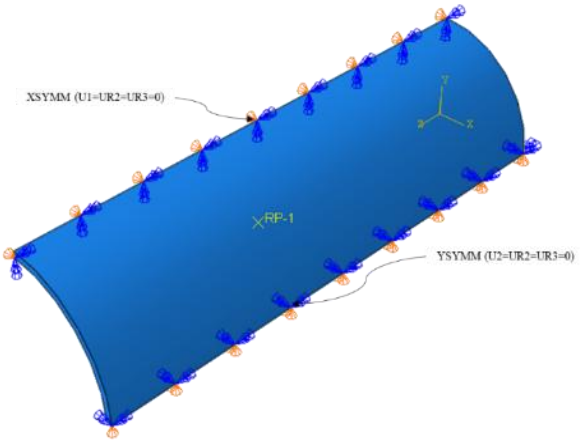

Fig. 12. Schematic of boundary conditions in ABAQUS/CAE software.

D. Scenario Variation

The scenario variations in the study were divided into physical and numerical parameter variations. Physical parameter variations were material variations. At the same time, the numerical parameter variations were mesh size variation and TNT loading variation. The TNT was placed at a distance of 400 mm, right in the middle of the open steel pipe. The mass of TNT that exploded was 0.6 kg and 0.8 kg. Table II shows a recapitulation of the simulation scenarios to be performed.

TABLE II. SIMULATION SCENARIO RECAP

Materials	Loading (kg)	Mesh (m)	Materials	Loading (kg)	Mesh (m)
API-5L-X42	0.6	0.0025	API-5L-X65	0.6	0.0025
		0.005			0.005
		0.0075			0.0075
		0.01			0.01
		0.0125			0.0125
		0.015			0.015
		0.0175			0.0175
		0.02			0.02
		0.0225			0.0225
		0.025			0.025
Cu-Ni 90/30	0.6	0.0025	Cu-Ni 70/30	0.6	0.0025
		0.005			0.005
		0.0075			0.0075
		0.01			0.01
		0.0125			0.0125
		0.015			0.015
		0.0175			0.0175
		0.02			0.02
		0.0225			0.0225
		0.025			0.025
HY-80	0.6	0.0025	HY-100	0.6	0.0025
		0.005			0.005
		0.0075			0.0075
		0.01			0.01
		0.0125			0.0125
		0.015			0.015
		0.0175			0.0175
		0.02			0.02
		0.0225			0.0225
		0.025			0.025
API-5L-X42	0.8	0.0025	API-5L-X65	0.8	0.0025
		0.005			0.005
		0.0075			0.0075
		0.01			0.01
		0.0125			0.0125
		0.015			0.015
		0.0175			0.0175
		0.02			0.02
		0.0225			0.0225
		0.025			0.025
Cu-Ni 90/30	0.8	0.0025	Cu-Ni 70/30	0.8	0.0025
		0.005			0.005
		0.0075			0.0075
		0.01			0.01
		0.0125			0.0125
		0.015			0.015
		0.0175			0.0175
		0.02			0.02
		0.0225			0.0225
		0.025			0.025
HY-80	0.8	0.0025	HY-100	0.8	0.0025
		0.005			0.005
		0.0075			0.0075
		0.01			0.01
		0.0125			0.0125
		0.015			0.015
		0.0175			0.0175
		0.02			0.02
		0.0225			0.0225
		0.025			0.025

1) Variation of material

In this research, material variations were applied to the object and simulated to compare existing models. There were six types of materials used to make open steel pipes, namely API-5L-X42 steel, API-5L-X65 steel, Copper-Nickel alloy (Cu-Ni 90/10), Copper-Nickel alloy (Cu-Ni 70/30), HY80 steel, HY100 steel. The material selection was based on laboratory trials conducted by Rushton [21] and materials that are often used in the steel pipe industry. The first material used was the same as used in the benchmarking reference, Mild steel. Mild steel is a type of low-carbon steel. The range depending on the amount of carbon varied depending on the source; 0.05%–0.25 % is the carbon range often found in mild steel. Examples of mild steel materials were API-5L-X42 and API-5L-X65. The properties of the materials can be seen in Table III.

TABLE III. MATERIAL PROPERTIES FOR API-5L-X42 AND API-5L-X65 BY RUSHTON [23] AND FATOBA [35]

Properties	Notation	X42	X65
Density (kg/m^3)	ρ	7850	7850
Young Modulus (GPa)	E	201	201
Poisson's Ratio (-)	v	0.28	0.3
Yield Stress (MPa)	σ_Y	290	290
Ultimate Tensile Stress (MPa)	σ	413.7	464
True Stress (MPa)	σ_T	500	580
True Strain (-)	ε_T	0.223	0.223

The following material used is Copper-Nickel alloys (Cu-Ni 90/10 and Cu-Ni 70/30). Copper-Nickel alloys are often encountered in marine-based industries, including thermal desalination, offshore oil and gas, power generation, and commercial and naval shipping. They have good resistance to corrosion and bio fouling in seawater and are easy to weld and fabricate. The main applications of Copper-Nickel Alloys are in seawater piping, heat exchangers, and condensers. Copper-nickel alloys are also used for hydraulic piping, including brake piping.

Two types of Copper-Nickel alloys are often used in the marine industry: Copper-Nickel 90/10 (Cu-Ni 90/10) and Copper Nickel 70/30 (CU-Ni 70/30). Cu-Ni 70/30 is more robust and has better resistance to seawater. Cu-Ni 90/10 tends to be more widely used in offshore applications due to its more affordable price with material quality that is not much different from Cu-Ni 70/30. Both alloys contain significant iron and manganese additions, making them suitable in terms of seawater flow resistance and overall corrosion. The material properties of Copper-Nickel alloys can be seen in Table IV.

TABLE IV. MATERIAL PROPERTIES FOR COPPER-NICKEL ALLOYS (CU-NI 90/10) AND (CU-NI 70/30) BY STEEL PIPE FACTORY [36]

Properties	Notation	Cu-Ni 90/10	Cu-Ni 70/30
Density (kg/m^3)	ρ	8940	8940
Young Modulus (GPa)	E	140	150
Poisson's Ratio (-)	v	0.223	0.223
Yield Stress (MPa)	σ_Y	372	454
Ultimate Tensile Stress (MPa)	σ	405.8	506.4
True Stress (MPa)	σ_T	507.25	633
True Strain (-)	ε_T	0.223	0.223

The last material used was HY steel. HY steel is a low alloy steel with high tensile strength and yield strength. Steel with enhanced strength has been used to build submarine hulls, whose structures are exposed to high loads caused by water pressure when submerged, impact when lying on the seabed, and the explosive effects of undersea mines and depth charges. The HY steel alloys often used by the United States after the world war are HY-80, HY-100, HY-130, and HY-200 steel [37].

HY-80 and HY-100 steels are low alloy steels where low alloy steels generally contain less than 8% non-ferrous elements, while high alloy steels contain more than 8% non-ferrous components. Both typically have mechanical properties that are superior compared to carbon steel. In 1970, HY steel material was developed by the United States Navy for use in ships, sub-Element, and exs [38]. The material properties of HY-80 and HY-100 steel can be seen in Table V.

TABLE V. MATERIAL PROPERTIES FOR HY-80 AND HY-100 STEEL BY HOLMQUIST [39]

Properties	Notation	HY80	HY100
Density (kg/m^3)	ρ	7750	7850
Young Modulus (GPa)	E	207	207
Poisson's Ratio (-)	v	0.3	0.3
Yield Stress (MPa)	σ_Y	550	784
Ultimate Tensile Stress (MPa)	σ	782	930
True Stress (MPa)	σ_T	977.5	862.5
True Strain (-)	ε_T	0.223	0.223

2) Variation of mesh size

The mesh size variation in this study was intended to determine the effect of mesh size on the accuracy of simulation data results in the finite element method. This variation was limited to the structural geometry used, namely the simulation validation structural geometry. The mesh arrangement in the open pipe structure model used eight-point Continum-3D solid elements with reduced integration (C3D8R). The open pipe was modeled with a wide range of meshing variations starting from 0.0025 m–0.025 m, increasing periodically by 0.0025 m.

VI. RESULTS AND DISCUSSION

After the blast simulation, the results were discussed in this section. Simulations were performed on each study variation. The results shown are in the form of plastic hoop strain, displacement, and von Mises stress.

A. Plastic Hoop Strain

The results taken from the simulation were the distribution and magnitude of the plastic hoop strain. From the distribution and magnitude of the stress, the strength of the structure in terms of material was analyzed, whether it was still within the safe limits of the yield criteria [40]. Table VI and Table VII show the results of plastic strain on the pipe structure after being subjected to blast loading with TNT loading of 0.6 kg and 0.8 kg.

TABLE VI. PLASTIC HOOP STRAIN WITH 0.6 KG TNT LOADING

Mesh / Material	0.0025	0.005	0.0075	0.01	0.0125	0.015	0.0175	0.02	0.0225	0.025
API-5L-X42	0.09303	0.0927	0.09152	0.09005	0.08754	0.08396	0.08104	0.07605	0.069253	0.06239
API-5L-X65	0.06268	0.06248	0.06207	0.06168	0.06043	0.05872	0.05761	0.05465	0.05064	0.04651
Cu-Ni 70/30	0.05849	0.05831	0.05797	0.05721	0.05628	0.05407	0.05278	0.04998	0.04601	0.04163
Cu-Ni 90/10	0.07454	0.07416	0.07353	0.0724	0.07084	0.06845	0.0661	0.06218	0.05716	0.05159
HY-100	0.03352	0.03342	0.03312	0.03291	0.03238	0.03157	0.0306	0.02747	0.02577	0.02293
HY-80	0.05034	0.05011	0.04982	0.04935	0.04882	0.04713	0.04556	0.04347	0.03986	0.0367

TABLE VII. PLASTIC HOOP STRAIN WITH 0.8 KG TNT LOADING

Mesh / Material	0.0025	0.005	0.0075	0.01	0.0125	0.015	0.0175	0.02	0.0225	0.025
API-5L-X42	0.1505	0.1497	0.1482	0.1455	0.1411	0.1348	0.1278	0.117	0.105	0.09415
API-5L-X65	0.1026	0.1022	0.1009	0.09931	0.09668	0.09265	0.09007	0.08496	0.0785	0.07243
Cu-Ni 70/30	0.09712	0.09687	0.09588	0.09504	0.09291	0.08929	0.08696	0.08177	0.07429	0.06764
Cu-Ni 90/10	0.119	0.1184	0.1172	0.1152	0.1129	0.1079	0.105	0.09852	0.08995	0.0814
HY-100	0.05942	0.05934	0.05884	0.05814	0.05747	0.05536	0.05391	0.05077	0.04624	0.04238
HY-80	0.07913	0.07892	0.07837	0.07794	0.07673	0.07448	0.0729	0.07	0.06499	0.06033

Based on the table above, the results showed that the final strain results between materials were similar. At 0.6 kg TNT loading, the highest strain value occurred at 0.0025 m mesh, and the lowest was at 0.025 m mesh in all materials. Following the theory described above, the smaller the mesh size used, the higher the convergence rate, and the more detailed and accurate the data obtained from meshing [41]. The following is the order of materials that had the highest to lowest strain values on a 0.0025 m mesh starting from API-5L-X42 at 0.09303, Cu-Ni 90/10 at 0.07454, API-5L-X65 at 0.06268, Cu-Ni 70/30 at 0.05849, HY-80 at 0.05034, and HY-100 at 0.03352. The strain values from highest to lowest at 0.025 m mesh started from API-5L-X42 at 0.06239, Cu-Ni 90/10 at 0.05159, API-5L-X65 at 0.04651, Cu-Ni 70/30 at 0.04163, HY-80 at 0.0367, and HY-100 at 0.02293. Fig. 13 compares the smallest and largest mesh plastic hoop strains that occurred in HY-100 material with 0.6 kg TNT loading. Images of plastic hoop strain at 0.6 kg TNT loading on API-5L-X42, API-5L-X65, Cu-Ni 70/30, Cu-Ni 90/10, and HY-80 materials are shown in Supplementary (Figs. S1–S5).

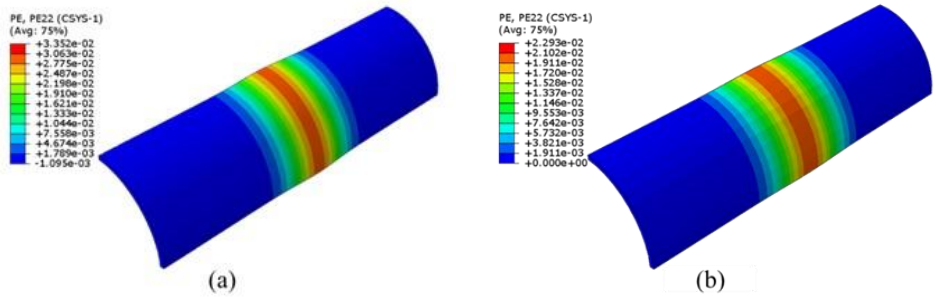

Fig. 13. Plastic hoop strain of HY-100 material loading 0.6 kg TNT (a) plastic hoop strain at mesh 0.0025 m, and (b) plastic hoop strain at mesh 0.025 m

At 0.8 kg TNT loading, the highest strain value occurred at 0.0025 m mesh, and the lowest was at 0.025 m mesh in all materials. The following is the sequence of materials that had the highest to lowest strain values at 0.0025 m mesh starting from API-5L-X42 at 0.1505, Cu-Ni 90/10 at 0.119, API-5L-X65 at 0.1026, Cu-Ni 70/30 at 0.09712, HY-80 at 0.07913, and HY-100 at 0.05942. The strain values from highest to lowest at 0.025 m mesh started from API-5L-X42 at 0.09415, Cu-Ni 90/10 at 0.0814, API-5L-X65 at 0.07243, Cu-Ni 70/30 at 0.06764, HY-80 at 0.06033, and HY-100 at 0.04238. Fig. 14 compares the smallest and largest mesh plastic hoop strains that occurred in HY-100 material with 0.8 kg TNT loading. Images of plastic hoop strain at 0.8 kg loading on API-5L-X42, API-5L-X65, Cu-Ni 70/30, Cu-Ni 90/10, and HY-80 materials are shown in Supplementary (Figs. S6–S10).

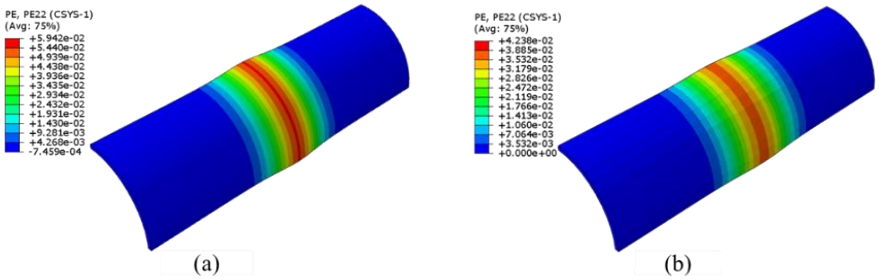

Fig. 14. Plastic hoop strain of HY-100 material loading 0.8 kg TNT (a) plastic hoop strain at mesh 0.0025 m, and (b) plastic hoop strain at mesh 0.025 m.

B. Displacement Behaviour

In this research, another output obtained was displacement. The ABAQUS/CAE software can also determine the displacement of the simulation model. The variation in this study was used to find the displacement value of each model. Table VIII and Table IX show the displacement of the pipe structure after being subjected to blast loading with 0.6 kg and 0.8 kg TNT loading.

TABLE VIII. DISPLACEMENT WITH 0.6 KG TNT LOADING

Mesh / Material	0.0025	0.005	0.0075	0.01	0.0125	0.015	0.0175	0.02	0.0225	0.025
API-5L-X42	0.01479	0.01476	0.01458	0.01438	0.014	0.01343	0.01302	0.01238	0.01149	0.0105
API-5L-X65	0.01005	0.01004	0.00998	0.00996	0.00988	0.00969	0.00954	0.00911	0.00954	0.0078
Cu-Ni 70/30	0.00906	0.00905	0.00899	0.00889	0.00876	0.00842	0.00824	0.00785	0.00738	0.00698
Cu-Ni 90/10	0.01174	0.0117	0.01163	0.01151	0.0113	0.01093	0.01055	0.00988	0.00907	0.00829
HY-100	0.00544	0.00542	0.00539	0.00534	0.0052	0.00498	0.00476	0.00425	0.00392	0.00339
HY-80	0.00823	0.0082	0.00817	0.00812	0.00804	0.00779	0.00759	0.00719	0.00659	0.00603

TABLE IX. DISPLACEMENT WITH 0.8 KG TNT LOADING

Mesh / Material	0.0025	0.005	0.0075	0.01	0.0125	0.015	0.0175	0.02	0.0225	0.025
API-5L-X42	0.02478	0.02467	0.02447	0.02403	0.02324	0.02217	0.02099	0.0193	0.01734	0.01568
API-5L-X65	0.01645	0.01639	0.01621	0.01599	0.01562	0.01506	0.01483	0.0143	0.01328	0.01229
Cu-Ni 70/30	0.01518	0.01516	0.01503	0.01493	0.01463	0.01412	0.01376	0.01295	0.01193	0.01095
Cu-Ni 90/10	0.01939	0.01932	0.01916	0.01883	0.01849	0.0177	0.01727	0.01626	0.01477	0.01332
HY-100	0.00977	0.00977	0.00971	0.00963	0.00953	0.0092	0.009	0.00843	0.00766	0.00694
HY-80	0.01278	0.01276	0.0127	0.0127	0.01261	0.01238	0.0122	0.0118	0.01098	0.01024

Based on the table above, the results showed that the final effect on TNT loading of 0.6 kg, the highest displacement value occurred on mesh 0.0025 m, and the lowest displacement value occurred on mesh 0.025 m on all materials. The following is the sequence of materials that have the highest to lowest displacement values on the 0.0025 m mesh starting from API-5L-X42 at 0.02478, Cu-Ni 90/10 at 0.01174, API-5L-X65 at 0.01005, Cu-Ni 70/30 at 0.00906, HY-80 at 0.00823, and HY-100 at 0.00544. The displacement value on the 0.025 m mesh from highest to lowest starts from API-5L-X42 at 0.0105, Cu-Ni 90/10 at 0.00829, API-5L-X65 at 0.0078, Cu-Ni 70/30 at 0.00698, HY-80 at 0.00603, and HY-100 at 0.00339. Fig. 15 compares the smallest and largest mesh displacement that occurred in HY-100 material with 0.6 kg TNT loading. Images of displacement at 0.6 kg loading of API-5L-X42, API-5L-X65, Cu-Ni 70/30, Cu-Ni 90/10, and HY-80 materials are shown in Supplementary (Figs. S11– S15).

At 0.8 kg TNT loading, the highest displacement value occurred at mesh 0.0025 m, and the lowest strain value appeared at mesh 0.025 m in all materials. The following is the sequence of materials that had the highest to lowest strain values on the 0.0025 m mesh starting from API-5L-X42 at 0.02478, Cu-Ni 90/10 at 0.01939, API-5L-X65 at 0.01645, Cu-Ni 70/30 at 0.01518, HY-80 at 0.01278, and HY-100 at 0.00977.

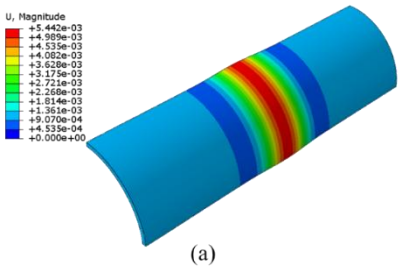

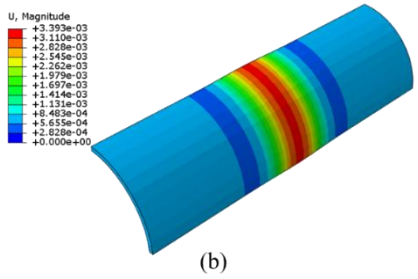

(b)

Fig. 15. Displacement of HY-100 material loading 0.6 kg TNT: (a) displacement at mesh 0.0025 m (b) displacement at mesh 0.025 m.

The displacement value on the 0.025 m mesh from highest to lowest started from API-5L-X42 at 0.01568, Cu-Ni 90/10 at 0.01332, API-5L-X65 at 0.01229, Cu-Ni 70/30 at 0.01095, HY-80 at 0.01024, and HY-100 at 0.00694. Fig. 16 compares the smallest and largest mesh displacement that occurs in HY-100 material with 0.8 kg TNT loading. Images of displacement at 0.8 kg loading of API-5L-X42, API-5L-X65, Cu-Ni 70/30, Cu-Ni 90/10, and HY-80 materials are shown in Supplementary (Figs. S16–S20).

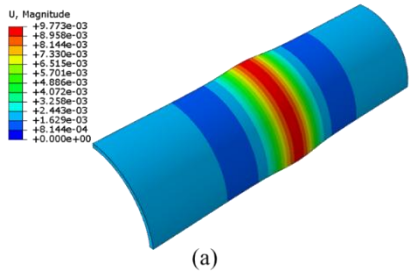

(a)

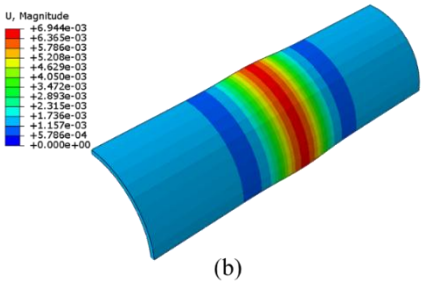

(b)

Fig. 16. Displacement of HY-100 material loading 0.8 kg TNT (a) displacement at mesh 0.0025 m, and (b) displacement at mesh 0.025 m.

C. *Von Mises Stress Contour*

The following result is the von Mises stress. The results showed that the cylindrical skin with red contours was part of the cylindrical skin that experienced the highest stress in the middle part where the TNT is detonated. The spread of blue and green contours was more dominant, so it did not experience significant stress. Fig. 17 shows the von Mises graph for each time interval in the material with 0.0025 m meshing. This study used a time interval setting of 100 in the ABAQUS application. In the ABAQUS CAE software, it is possible to define a set of arbitrary time points and request a field or history output for each time point in the group. This option makes it possible to create customized output frequencies to order output during critical periods in the analysis as required s. Each time interval defines the von Mises stress value at the cylinder shell in this case. The time intervals were 0, 25, 50, 75, and 100. At a meshing setting of 0.0025 m, the highest stress occurred in the HY-100 material (Supplementary, Fig. S24) at interval 50, which is 800.4 MPa. The minor stress at 0.0025 m meshing setting occurred in API-5L-X42 material at a time interval 25 of 346.4 MPa. The color distribution contours on API-5L-X42 material meshing 0.0025 m and on other materials can be seen in Fig. 18 and Supplementary (Figs. S21–S25).

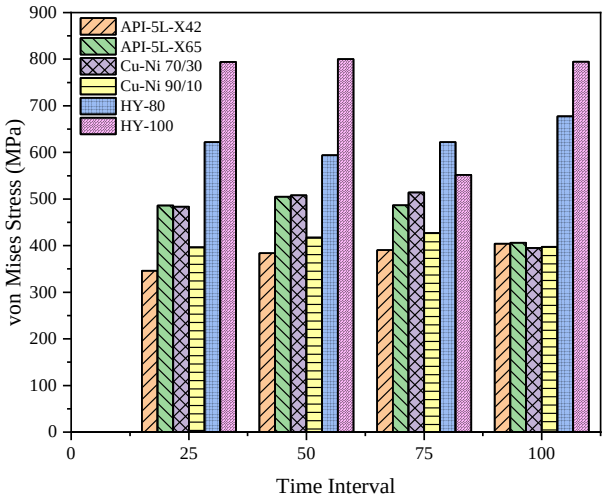

Fig. 17. Von Mises stress graph for each time interval at 0.0025 m meshing.

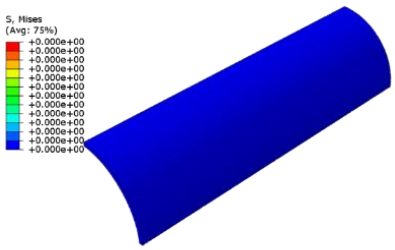

(a)

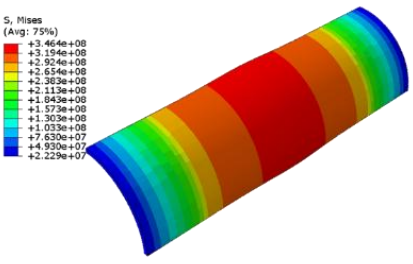

(b)

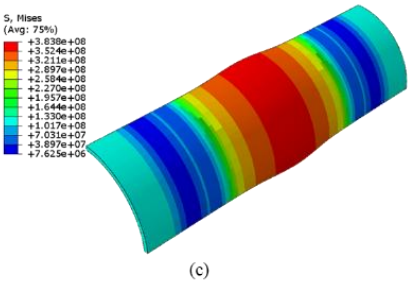

(c)

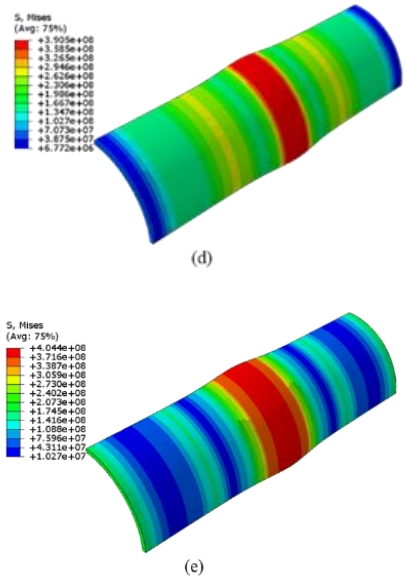

Fig. 18. Von Mises stress contours of 0.0025 m meshing in API-5L-X42 material at each time interval (a) 0, (b) 25, (c) 50, (d) 75, and (e) 100.

At 0.0125 m meshing setting, the highest stress occurred in HY-100 material (Supplementary–Fig. S29) at interval 50, which was 798.4 MPa. The minor stress at 0.0125 m meshing setting occurred in API-5L-X42 material at a time interval 25 of 345.2 MPa. Fig. 19 shows the von Mises graph for each time interval in the material with 0.0125 m meshing. The color distribution contours of API-5L-X42 material with 0.0125 m meshing and other materials can be seen in Fig. 20 and Supplementary (Figs. S26–S30).

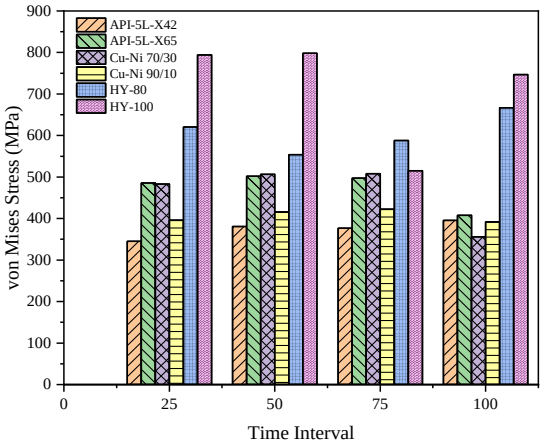

Fig. 19. Von Mises stress graph for each time interval at 0.0125 m meshing.

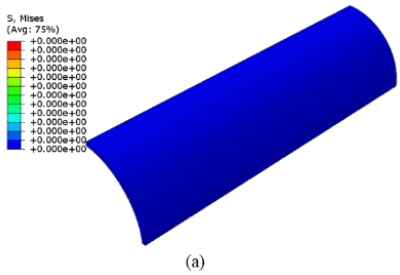

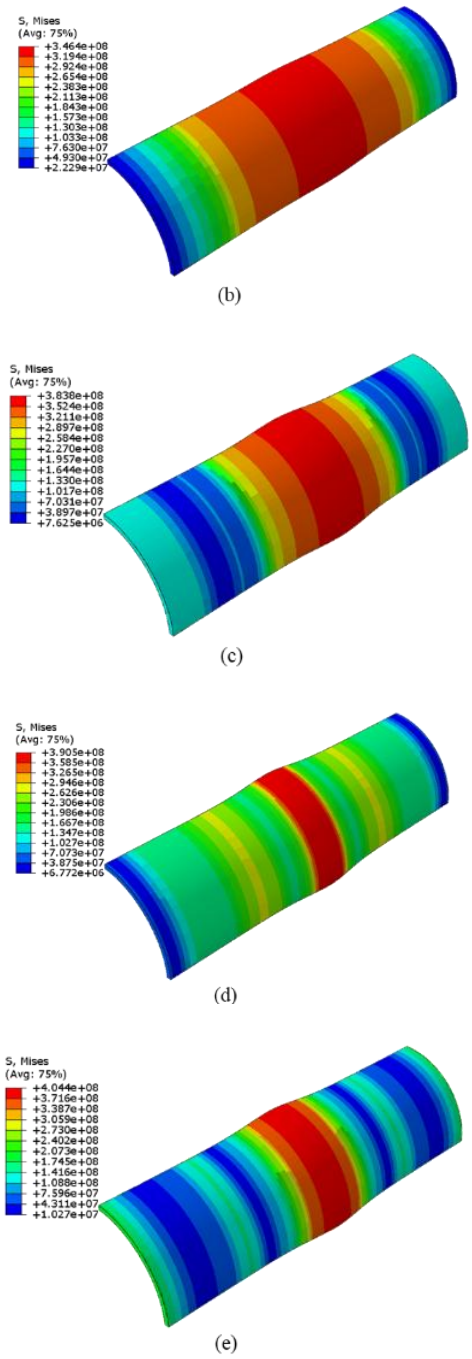

Fig. 20. Von Mises stress contours of 0.0125 m meshing in API-5L-X42 material at each time interval (a) 0, (b) 25, (c) 50, (d) 75, and (e) 100.

At a meshing setting of 0.0250 m, the highest stress occurred in the HY-100 material (Supplementary–Fig. S34) at a time interval of 25 which is 791.7 MPa. The minor stress at 0.0250 m meshing setting appears in the Cu-Ni 90/30 material at a time interval 100 of 257.7 MPa. Fig. 21 shows the von Mises graph for each time interval in the material with 0.0250 m meshing. The color distribution contours of API-5L-X42 material with 0.0250 m meshing and other materials can be seen in Fig. 22 and Supplementary (Figs. S31–S35).

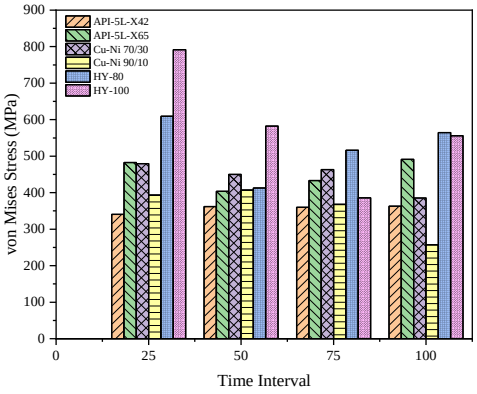

Fig. 21. Graph of von Mises stresses at each time interval at 0.0250 m meshing.

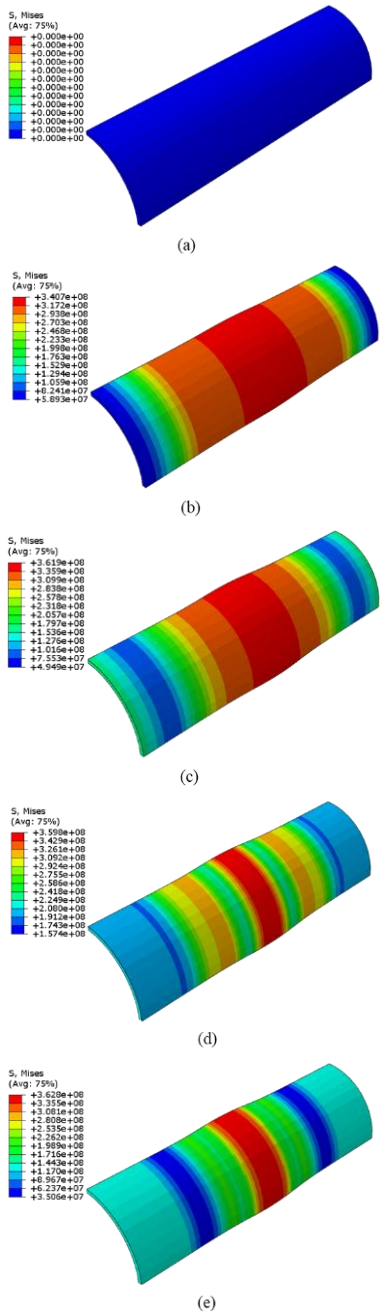

Fig. 22. Von Mises stress contours of 0.0250 m meshing in API-5L-X42 material at each time interval (a) 0, (b) 25, (c) 50, (d) 75, and (e) 100.

VII. Conclusions

A steel pipe-shaped structure is a closed leak-proof container designed to hold liquids or gases at pressures different from ambient pressure. This research was conducted with several material variations, namely API-5L-X42, API-5L-X65, Cu-Ni 70/30, Cu-Ni 90/10, HY-100, and HY-80 to determine the performance of the steel pipe-shaped structure after being subjected to a TNT blast loading positioned in the center of the steel pipe-shaped structure. Tests were conducted using the CONWEP method in ABAQUS with air blasts with TNT loads of 0.6 kg and 0.8 kg. The meshing part is crucial in finite element simulation. In this study, meshing variations were carried out with a size of 0.0025 m–0.025 m, gradually increasing by 0.0025 m. Based on the simulation results, the following conclusions can be drawn:

- The simulation results showed the structural ability of each variation to withstand different air blast loads. Based on the simulation results, it was found that the best material for steel pipe-shaped structure was HY-100. The smaller the mesh size, the higher the convergence rate, so the data obtained from meshing will be more detailed and accurate. The greater the loading on TNT, the results of displacement, plastic hoop strain, and stress also increase.
- The displacement and plastic hoop strain values with 0.6 kg and 0.8 kg TNT loading in this simulation showed that HY100 material had the lowest value among other materials due to its high tensile strength. The higher the tensile strength value of a material, the higher the hardness level. The maximum von Mises stress values in the steel pipe-shaped structure simulation reached 800.4, 798.4, and 791.7 MPa for meshing of 0.0025 m, 0.0125 m, and 0.0250 m, respectively.

Based on the results and experience of this study, the researcher suggests further research on these variations with simulation methods by varying the geometry again. Many other geometry models can represent future research opportunities to create steel pipe-shaped structure structures with better performance.

Conflict of Interest

The authors declare no conflict of interest.

Author Contributions

MIM conducted formal analysis, conducted validation, and conducted writing - original draft; ARP designed methodology, conducted supervision, managed project administration; obtained funding acquisition, conducted data curation, and conducted writing - review & editing; TM designed methodology, conducted conceptualization, conducted conceptualization, and conducted writing - review & editing; NM conducted supervision, conducted conceptualization, and managed project administration; QTD designed methodology, and conducted conceptualization; MIH checked visualization, and managed software; MRAP checked visualization, and

conducted writing-original draft; all authors had approved the final version.

REFERENCES

[1] Indonesian Iron and Steel Industry Association, "National Steel Industry for Advanced Indonesia," IISIA Business Forum 2022, 2022.

[2] I. Ahmad and M. Fahri, "The role of the indonesian steel industry in supporting the indonesia defense industry," *Nationalism dan Integrity*, vol. 7, no. 3, pp. 2549–9459, 2021.

[3] A. R. Prabowo, T. Tuswan, R. Adiputra, Q. T. Do, J. M. Sohn, E. Surojo, F. Imaduddin, "Mechanical behavior of thin-walled steel under hard contact with rigid seabed rock: Theoretical contact approach and nonlinear FE calculation," *Journal of the Mechanical Behavior of Materials*, vol. 30, no. 1, pp. 156–170, Jan. 2021.

[4] A. R. Prabowo, D. M. Bae, and J. M. Sohn, "Comparing structural casualties of the Ro-Ro vessel using straight and oblique collision incidents on the car deck," *Journal of Marine Science and Engineering*, vol. 7, no. 6, article no. 183, 2019.

[5] A. R. Prabowo, Q. T. Do, B. Cao, and D. M. Bae, "Land and marine-based structures subjected to explosion loading: A review on critical transportation and infrastructure," *Procedia Structural Integrity*, vol. 27, pp. 77–84, 2020

[6] Q. T. Do, T. Muttaqie, P. T. Nhut, M. T. Vu, N. D. Khoa, and A. R. Prabowo, "Residual ultimate strength assessment of submarine pressure hull under dynamic ship collision," *Ocean Engineering*, vol. 266, article no. 112951, 2022.

[7] I. Widiyanto, A. R. Prabowo, T. Muttaqie, N. Muhayat, I. Yaningsih, D. D. D. P. Tjahjana, W. E. Juwana, T. Miyazaki, "Effects of geometry and material factors on the behavior of stiffened offshore pipe structures under hydrostatic pressure," *Journal of Applied Engineering Science*, vol. 20, no. 4, pp. 1103–1121, 2022.

[8] D. T. A. Ansori, A. R. Prabowo, T. Muttaqie, N. Muhayat, F. B. Laksono, D. D. D. P. Tjahjana, A. Prasetyo, and Y. Kuswardi, "Investigation of honeycomb sandwich panel structure using aluminum alloy (AL6XN) material under blast loading," *Civil Engineering Journal*, vol. 8, no. 5, pp. 1046–1068, 2022.

[9] M. A. H. Mubarok, T. Muttaqie, A. R. Prabowo, J. M. Sohn, E. Surojo, and F. Imaduddin, "Effects of geometrical variations on the performance of hull plate structures under blast load: A study using nonlinear FEA," *Procedia Structural Integrity*, vol. 41, pp. 282–289, 2022.

[10] M. Lackner, F. Winter, and A. K. Agarwal, *High Energy Materials (Propellants, Explosives, and Pyrotechnics)*, John Wiley & Sons, 2010.

[11] C. Beyle, C. Wissinger, P. Crombie, C. Connealy, M. Goodson, J. Lentini, M. Robin, "Strengthening fire and explosion investigation in the United States: A strategic vision for moving forward," 2021.

[12] U. EPA, "Technical Fact Sheet–2,4,6-Trinitrotoluene (TNT)," 2014.

[13] K. Chi, J. Li, and C. Wu, "Numerical simulation of buried steel pipelines subjected to ground surface blast loading," *Thin-Walled Structures*, vol. 186, 2023.

[14] T. Wu, N. Jiang, C. Zhou, X. Luo, H. Li, and Y. Zhang, "Experimental and numerical investigations on damage assessment of high-density polyethylene pipe subjected to blast loads," *Engineering Failure Analysis*, vol. 131, article no. 105856, 2022.

[15] B. S. Elveli, O. Vestrum, K. O. Hauge, T. Berstad, T. Børvik, and V. Aune, "Thin steel plates exposed to combined ballistic impact and partially confined airblast loading," *Engineering Failure Analysis*, vol. 144, article no. 106943, 2023.

[16] K. Song, Y. Long, C. Ji, F. Gao, and H. Chen, "Experimental and numerical studies on the deformation and tearing of X70 pipelines subjected to localized blast loading," *Thin-Walled Structures*, vol. 107, pp. 156–168, 2016.

[17] T. F. Henchie, S. Chung Kim Yuen, G. N. Nurick, N. Ranwaha, and V. H. Balden, "The response of circular plates to repeated uniform blast loads: An experimental and numerical study," *International Journal of Impact Engineering*, vol. 74, pp. 36–45, 2014.

[18] D. Karagiozova, G. N. Nurick, and S. C. K. Yuen, "Energy absorption of aluminium alloy circular and square tubes under an axial explosive load," *Thin-Walled Structures*, vol. 43, no. 6, pp. 956–982, 2005.

[19] H. Zhu, X. Wang, Y. Wang, G. Wu, Y. Cao, and C. Ji, "Dynamic responses of aluminum alloy plates coated with polyurea elastomer subjected to repeated blast loads: Experimental and numerical investigation," *Thin-Walled Structures*, vol. 189, 2023.

[20] M. Kristoffersen, K. O. Hauge, A. Minoretti, and T. Børvik, "Experimental and numerical studies of tubular concrete structures subjected to blast loading," *Engineering Structures*, vol. 233, 2021.

[21] Y. Sun, D. Ryumin, I. Kagirov, A. Axyonov, N. Pavlyuk, A. Saveliev, I. Kipyatkova, M. Zelezny, I. Mporas, and A. Karpov, "Damage effect of steel circular tube subjected to fire and blast," *Journal of Constructional Steel Research*, vol. 176, 2021.

[22] G. Patnaik and A. Rajput, "Safety assessment of underground steel pipelines with CFRP protection against subsurface blast loading," *Structures*, vol. 54, pp. 1541–1559, 2023.

[23] N. Rushton, G. K. Schleyer, A. M. Clayton, and S. Thompson, "Internal explosive loading of steel pipes," *Thin-Walled Structures*, vol. 46, no. 7–9, pp. 870–877, 2008.

[24] Government of Western Australia, *Pipe Fabrication Materials, Drawing and Fabrication Methods Metals and Engineering ENG2068*, 2016. [Online]. Available: www.dtwd.wa.gov.au

[25] J. Lee, T. E. Lacy, and C. U. Pittman, "Lightning mechanical damage prediction in carbon/epoxy laminates using equivalent air blast overpressure," *Composites Part B: Engineering*, vol. 212, article no. 108649, 2021.

[26] W. A. Lyons and E. R. Williams, "Atmospheric electricity and lightning," in *Handbook of Weather, Climate, and Water*, John Wiley & Sons, Inc., 2004, pp. 407–431.

[27] J. Lee, T. E. Lacy, C. U. Pittman, and J. N. Reddy, "Numerical estimations of lightning-induced mechanical damage in carbon/epoxy composites using shock wave overpressure and equivalent air blast overpressure," *Composite Structures*, vol. 224, article no. 111039, 2019.

[28] F. G. Friedlander, "The diffraction of sound pulses I. Diffraction by a semi-infinite plane," in *Proc. the Royal Society of London. Series A. Mathematical and Physical Sciences*, vol. 186, no. 1006, 1946, pp. 322–344.

[29] K. Lahiri and L. Ho, "Simulation of rapid structural failure due to blast loads from conventional weapons (CONWEP)," in *Proc*. the NAFEMS World Congress, 2011.

[30] Z. Huang, L. Gao, Y. Wang, and F. Wang, "Determination of the Johnson-Cook constitutive model parameters of materials by cluster global optimization algorithm," *Journal of Materials Engineering and Performance*, vol. 25, no. 9, pp. 4099–4107, 2016.

[31] F. H. A. Alwan, A. R. Prabowo, T. Muttaqie, N. Muhayat, R. Ridwan, and F. B. Laksono, "Assessment of ballistic impact damage on aluminum and magnesium alloys against high velocity bullets by dynamic FE simulations," *Journal of the Mechanical Behavior of Materials*, vol. 31, no. 1, pp. 595–616, 2022.

[32] F. Maulana, A. R. Prabowo, R. Ridwan, U. Ubaidillah, D. Ariawan, J. M. Sohn, N. Muhayat, D. D. D. P. Tjahjana, and Q. T. Do, "Antiballistic material, testing, and procedures of curved-layered objects: A systematic review and current milestone," *Curved and Layered Structures*, vol. 10, no. 1, article no. 20220200, 2023.

[33] A. A. Pratama, A. R. Pratama, T. Muttaqie, N. Muhayat, R. Ridwan, B. Cao, and F. B. Laksono, "Hollow tube structures subjected to compressive loading: Implementation of the pitting corrosion efect in nonlinear FE analysis," *Journal of the Brazilian Society of Mechanical Sciences and Engineering*, vol. 45, article no. 143, 2023.

[34] A. R. Prabowo, R. Ridwan, T. Tuswan, and F. Imaduddin, "Forecasting the effects of failure criteria in assessing ship structural damage modes," *Civil Engineering Journal*, vol. 8, no. 10, pp. 2053–2068, 2022.

[35] O. Fatoba and R. Akid, "Low cycle fatigue behaviour of API 5L X65 pipeline steel at room temperature," *Procedia Engineering*, vol. 74, pp. 279–286, 2014.

[36] S. P. Factory, "Datasheet for copper nickel," [Online]. Available: https://www.steelpipesfactory.com/ [Online; accessed: 28-March-2023].

[37] S. Bogdan and K. Radosław, "Material properties of hy 80 steel after 55 years of operation for FEM applications," *Materials*, vol. 14, no. 15, p. 4213, 2021.

[38] M. F. Ashby and D. Cebon, "Materials selection in mechanical design," *Le Journal de Physique IV*, vol. 3, no. C7, pp. C7-1, 1993.

[39] J. Holmquist, "Strength and fracture characteristics of HY-80, HY-100, and HY-130 steels subjected to various strains, strain rates,

temperatures, and pressures," Washington Navy Yard, DC: Naval Surface Warfare Center, pp. 99–252, 1987.
[40] T. Wierzbicki and W. Abramowicz, "On the crushing mechanics of thin-walled structures," *Journal of Applied Mechanics*, vol. 50, no. 4a, pp. 727–734, 1983.
[41] Dassault Systèmes, "Getting started with ABAQUS: Interactive edition 6.12," Getting Started with ABAQUS: Interactive Edition, pp. 4–50, 2012.